

Towards quantum networks of single spins: analysis of a quantum memory with optical interface in diamond

Journal:	<i>Faraday Discussions</i>
Manuscript ID:	FD-ART-06-2015-000113
Article Type:	Paper
Date Submitted by the Author:	23-Jun-2015
Complete List of Authors:	Blok, Machiel; QuTech, Delft University of Technology Kalb, Norbert; QuTech, Delft University of Technology Reiserer, Andreas; QuTech, Delft University of Technology Taminiau, Tim Hugo; QuTech, Delft University of Technology Hanson, Ronald; QuTech, Delft University of Technology

Towards quantum networks of single spins: analysis of a quantum memory with optical interface in diamond

M.S. Blok^{1,†}, N. Kalb^{1,†}, A. Reiserer¹, T.H. Taminiau¹ and R. Hanson^{1,*}

¹*QuTech and Kavli Institute of Nanoscience, Delft University of Technology,
PO Box 5046, 2600 GA Delft, The Netherlands*

[†]*These authors contributed equally to this work*

** corresponding author: r.hanson@tudelft.nl*

Abstract

Single defect centers in diamond have emerged as a powerful platform for quantum optics experiments and quantum information processing tasks¹. Connecting spatially separated nodes via optical photons² into a quantum network will enable distributed quantum computing and long-range quantum communication. Initial experiments on trapped atoms and ions as well as defects in diamond have demonstrated entanglement between two nodes over several meters³⁻⁶. To realize multi-node networks, additional quantum bit systems that store quantum states while new entanglement links are established are highly desirable. Such memories allow for entanglement distillation, purification and quantum repeater protocols that extend the size, speed and distance of the network⁷⁻¹⁰. However, to be effective the memory must be robust against the entanglement generation protocol, which typically must be repeated many times. Here we evaluate the prospects of using carbon nuclear spins in diamond as quantum memories that are compatible with quantum networks based on single nitrogen vacancy (NV) defects in diamond. We present a theoretical framework to describe the dephasing of the nuclear spins under repeated generation of NV spin-photon entanglement and show that quantum states can be stored during hundreds of repetitions using typical experimental coupling parameters. This result demonstrates that nuclear spins with weak hyperfine couplings are promising quantum memories for quantum networks.

1 Introduction

1.1 The NV-center as a quantum node

Spins associated with the nitrogen-vacancy (NV) center, an atomic defect in diamond, have recently emerged as a promising platform for quantum networks^{1,11}. The NV-center's long-lived electron spin state ($S=1$) can be controlled by magnetic resonance and can be initialized and read out optically. At cryogenic temperatures (< 10 K), coherent optical transitions allow for the generation of spin-photon entanglement¹² and of entanglement between spatially separated NV center electron spins^{6,13}.

In addition, the electron spin couples to nuclear spins in the environment through the hyperfine interaction. Control over the host nitrogen spin and over multiple nearby ^{13}C spins has been demonstrated¹⁴⁻²⁰. As these nuclear spins can be well isolated from their environments, coherence times of more than one second have been demonstrated²¹, making them interesting candidates for quantum network memories.

1.2 Combining a quantum memory with an optical interface

A major challenge for realizing quantum memories based on nuclear spins is to overcome the dephasing that is introduced while using the electron spin as an optical interface to generate spin-photon entanglement. Consider the general case of an entanglement protocol that is inherently probabilistic due to lossy optical channels. The protocol therefore must be repeated many times in order to establish an entanglement link between adjacent network nodes. Whenever the entanglement attempt fails, the electron spin is projected in a random state. A fast and practical solution is to re-initialize the spin by optical pumping after each repetition. Because the exact time at which the electron spin is reset is uncertain (optical pumping is a stochastic process) and the electron-nuclear interaction is always present, the electron reset can cause nuclear spin dephasing (Fig 1). A promising route to overcome this dephasing of the quantum memory is to use relatively distant ^{13}C spins with weak hyperfine couplings, which are less sensitive to fluctuations of the electron spin.

In this manuscript we explore the storage of quantum states in ^{13}C spins during the repeated generation of NV spin-photon entanglement. We first demonstrate a method to directly measure the frequency difference df for the electron-state-dependent nuclear spin precessions, which governs the nuclear dephasing (Fig 1)²². We then analyze the spin-photon entanglement protocol, develop a model to describe the dephasing of nuclear spins, and calculate the fidelity of nuclear spin quantum memories with realistic coupling parameters under many repetitions of the entanglement protocol.

2 Control and characterization of nuclear spins in diamond

We start by discussing the experimental methods to control the NV center and nearby ^{13}C nuclear spins. We then introduce a Ramsey-spectroscopy method to directly determine the frequency df and characterize four candidate ^{13}C spins near a single NV-center. These experimental results highlight the universal presence of controllable nuclear spin memories and provide a realistic set of input parameters for the theoretical calculations.

2.1 Setup and electron spin control

At the heart of the experiment is a single Nitrogen-Vacancy (NV) center in high purity (Type IIa) single-crystal diamond grown by chemical-vapor-deposition. The diamond is held at a temperature of $T = 4.2$ K in a Helium bath cryostat. The diamond has a natural abundance (1.1%) of ^{13}C spins ($I = 1/2$) in an otherwise ^{12}C spin-free lattice. The NV electronic spin is polarized and measured optically by spin-selective resonant excitation^{12,23,24}. To obtain high single-shot readout fidelities, a solid-immersion lens was fabricated on top of the NV center and a single-layer aluminum-oxide anti-reflective coating was deposited¹³ (Fig 1). The electronic spin is controlled by microwaves applied through an on-chip line (Rabi frequency: 3.3 MHz).

2.2 Carbon spin control by dynamical decoupling

We detect and control multiple ^{13}C nuclear spins in the spin bath surrounding the NV center using recently developed methods that coherently exploit the electron-nuclear interaction by periodically switching the electron state at well-defined times^{20,25-27}. We apply sequences of the form $(\tau - \pi - 2\tau - \pi - \tau)^{M/2}$, where π denotes a microwave pulse that rotates the electron by 180 degrees, 2τ is the interpulse delay and M the total number of π -pulses. For τ precisely resonant with the electron-nuclear dynamics, this sequence imprints a phase on the electron spin conditional on the nuclear spin state.

Because the hyperfine interaction is determined by the specific position of each nuclear spin relative to the NV center, the resonance condition for τ is different for each nuclear spin. We can thus characterize the nuclear spin environment²⁰ by preparing the electron in a superposition state and measuring the phase that is acquired when sweeping τ . Here we select four individual ^{13}C spins to study in more detail, and design controlled gates following Taminiau et al.²⁷.

2.3 Characterization of single nearby nuclear spins

The nuclear spin dynamics are characterized by the nuclear spin precession frequencies ω_0 and ω_1 corresponding to the electron spin being in $m_s=0$ and $m_s=1$, respectively (see also Methods). To directly determine the frequencies ω_0 , ω_1 and $df=(\omega_1 - \omega_0)/2\pi$ for each of the four nuclear spins we perform the experimental sequence²² shown in Fig 2a. The electron is prepared in state $\rho_{0,e} = |0\rangle\langle 0|$, whereas the nuclear spin state is un-polarized (mixed state $\rho_{m,c} = (|0\rangle\langle 0| + |1\rangle\langle 1|)/2$). The first set of gates correlates the electron state with the X-projection of the nuclear spin state, so that the state is $\rho_{0,e} \otimes \rho_{x,c} + \rho_{1,e} \otimes \rho_{-x,c}$, with $\rho_{\pm x,c} = |\pm X\rangle\langle \pm X|$ and $|\pm X\rangle = (|0\rangle_c \pm |1\rangle_c)/\sqrt{2}$. The controlled nuclear spin rotations are realized by the pulse sequences described above, with τ resonant for that specific spin. Second, the nuclear spin evolves freely, either with ω_0 or with ω_1 , depending on the electron state. Finally the phase accumulation of the nuclear spin is measured by correlating it to the electron spin before reading out the electron spin.

The beating observed in the signal directly yields the frequency difference df and therefore the additional phase picked up due to the time the electron spent in $m_s = +1$. For the four spins we find $df = (29.6 \pm 0.6)$, (-32.2 ± 0.3) (38.6 ± 0.2) and (45.6 ± 0.6) kHz respectively. These values show that several nuclear spins with coupling strengths between approximately 20-50 kHz are readily available in diamond samples with a natural abundance of ^{13}C .

3 Modelling the dephasing of a carbon spin during entanglement generation

3.1 Sequence for generating heralded entanglement

We analyze the performance of ^{13}C spins as quantum memory in the context of the heralded entanglement protocol proposed by Barrett and Kok²⁸, which was implemented by Bernien et al.⁶. The protocol is based on the creation of spin-photon entanglement at both nodes, followed by two-photon interference and measurement of these photons. The protocol is probabilistic since it is susceptible to photon loss. Importantly, successful generation of entanglement is heralded by the detection of the two photons and thus the sequence can be repeated until successful.

Spin-photon entanglement is created using the following sequence. The electron spin is prepared in state $|0\rangle_e$ by optical pumping (Fig 3). Using microwaves the electron spin is then brought in a coherent superposition. Next, the NV center is optically excited with a short laser pulse that is only resonant if the spin is in state $|0\rangle_e$. Spontaneous emission generates a photon that is entangled with the state of the spin: $|\Psi\rangle = 1/\sqrt{2}(|0\rangle_e|1\rangle_p + |1\rangle_e|0\rangle_p)$ where $|1\rangle_p$ ($|0\rangle_p$) denotes the presence (absence) of a photon. The goal is that the nuclear spin memory reliably stores quantum states during many repetitions of this sequence.

3.2 Evolution of carbon spin while generating entanglement

The performance of a quantum memory can be characterized by its ability to store an unknown quantum state $|\psi\rangle = \alpha|0\rangle_c + \beta e^{i\varphi}|1\rangle_c$. During the spin-photon entanglement sequences the phase φ of the nuclear spin state is affected

in two ways. First, when the emitted photon is lost (heralding fails), the electron spin state is randomly projected into either $|0\rangle_e$ or $|1\rangle_e$ resulting in nuclear spin evolutions with ω_0 or ω_1 , respectively. Second, before the next repetition, the electron spin is reset by optical pumping, a stochastic process that introduces a distribution of spin flip times. These two effects are now analyzed separately.

After a single round of optical excitation that generates spin-photon entanglement, the electron spin is projected into an unknown eigenstate if the photon is lost. The carbon spin acquires a phase $d\omega t$ if the electron is projected in $|1\rangle_e$, where $d\omega = 2\pi df$ and t the time at which the reset is applied. When this process is repeated N times, the number of times k that the electron is projected in $|1\rangle_e$ is given by a binomial distribution and the final state fidelity F of the carbon spin state is given by:

$$F = \frac{1}{2} + \frac{1}{2^{N+1}} \sum_{k=0}^N \binom{N}{k} \cos[k d\omega t] \quad (3.1)$$

where the electron spin reset is taken to be instantaneous and we only consider the initial memory state is $|\psi\rangle = 1/\sqrt{2}(|0\rangle_c + |1\rangle_c)$, which is most sensitive to dephasing. Fig 3b shows the calculated fidelity as a function of the time t , for two carbon spins that were identified in Fig 2. For each carbon spin there is a unique condition at $t = 2\pi / d\omega$, for which the phase is independent on the electron state resulting in $F=1$. Note that in the full entanglement protocol^{6,28} an electron π -pulse is applied between rounds of excitation, so that this phase difference can be cancelled for all t .

In reality the reset of the electron spin by spin pumping is a stochastic process involving multiple transitions to the optically excited state as well as mixing between multiple excited states. Here we model the dynamics of this process as an exponential distribution $e^{-\frac{t'}{\tau_{reset}}}$ with a characteristic time τ_{reset} . In Fig 3c we compare the results of a monte-carlo simulation that includes the probabilistic reset time t' for $\tau_{reset} = 390 \text{ ns}$ with the curve of equation (3.1). As expected the

same behavior is observed, but the maximum fidelity is reduced since the stochastic reset leads to dephasing of the carbon spin.

3.3 Dephasing of the memory including spin pumping

To analyze the effect of the electron spin reset on the nuclear spin in detail we now assume that $t = 2\pi / d\omega$ which allows us to derive an analytical expression for the fidelity of the carbon spin (see methods for the derivation of this result):

$$F = \frac{1}{2} + \frac{1}{2^{N+1}} \left(1 + e^{-\frac{1}{2}\tau_{reset}^2 d\omega^2} \right)^N \quad (3.2)$$

In Fig 3d we plot the resulting memory fidelity after 250 entanglement repetitions versus the reset constant τ_{reset} , for different values of df . Although for an instantaneous reset ($\tau_{reset} \rightarrow 0$) the state can be perfectly preserved, a finite uncertainty in the reset time constant reduces the fidelity, with the effect being stronger for higher coupling strengths df . A natural lower limit to the reset time τ_{reset} is the slowest decay rate involved in the spin pumping process. For the NV center this is expected to be the singlet lifetime $\tau_{singlet} \approx 390 \text{ ns}$ ²⁹. For this value, Fig 3d predicts that for coupling strengths of $df < 10 \text{ kHz}$ the state can be preserved with a fidelity of $> 98 \%$ even after 250 entanglement attempts.

The reset constants currently reported in the literature are approximately $1 \mu\text{s}$ ⁶. In Fig 3e we plot the fidelity as a function of number of entanglement attempts for $\tau_{reset} = 1 \mu\text{s}$. These calculations predict that 25 repetitions of the entanglement protocol will yield a fidelity of 90.3 % for the lowest coupling strength found in Fig 2, which would already provide significant speed advantages in establishing entanglement links⁸. For coupling strengths $df < 10 \text{ kHz}$, hundreds of repetitions become feasible. Such lower coupling strengths are available in isotopically purified diamonds²¹.

We emphasize that the model presented here does not include the detailed excited state dynamics of the spin pumping process. We expect that averaging over rapid spin flips and time spent in states with zero spin projection during

these dynamics will further reduce actual dephasing. We therefore expect that our analysis sets a lower bound for the number of possible repetitions.

4. Conclusions

We have modelled the dephasing of nuclear spins quantum memories coupled to an NV electron spin that is repeatedly used to establish spin-photon entanglement. We find that nuclear spins with weak hyperfine couplings (20-50 kHz) are readily available in natural abundance diamonds. Our analysis shows that these spins can be used to store quantum states during 25 entanglement attempts with a fidelity of 90.3%, while nuclear spins in isotopically purified samples with coupling strengths below 10 kHz can even enable hundreds of repetitions. These results demonstrate that nuclear spins with weak hyperfine coupling strengths are promising quantum memories for quantum networks providing a route towards entanglement distillation and quantum repeaters.

5. Methods

5.1 analytical derivation including the stochastic repumping process

We take the limit of $\gamma_C B \gg A_\perp$ (with A_\perp the hyperfine component perpendicular to the static magnetic field) such that the eigenstates of the ^{13}C -spin are independent of the electron and the only net effect of the electron-carbon coupling is that the carbon acquires a phase depending on the state of the electron. Choosing the rotating frame of the carbon resonant with the energy splitting for the electron in $|0\rangle_e$, the carbon state will acquire a phase $e^{i d \omega t}$ for the electron in $|1\rangle_e$ (with $d\omega = 2\pi df$) and does not evolve otherwise.

We derive an expression for the maximally achievable memory fidelity. The scheme of Fig 3a is repeated N times. Phase errors occur if the electron spin has to be reinitialized by pumping it to another spin state. During every execution of the protocol, the electron spin is projected into $|0\rangle_e$ or $|1\rangle_e$ with equal probability. The probability for k repumping events is then given by a binomial distribution

$$P_{ek} = \frac{1}{2^N} \binom{N}{k} \quad (5.1)$$

Every time the electron is reset from $|1\rangle_e$ into $|0\rangle_e$ the memory spin will pick up a random phase $\delta\theta = d\omega (t' - \tau_{reset})$ which is given by the difference between energy levels of the carbon spin conditional on the electron spin $d\omega$ and the deviation $(t' - \tau_{reset})$ from the mean repumping time. The overall acquired phase for k repumping events is then the sum of the individual random phases. The fidelity with the initial memory state after N repetitions is thus given by

$$F_k = \frac{1}{2} (1 + \cos[\sum_{k=0}^N \delta\theta]) \quad (5.2)$$

Under the assumption that the distributions for all repumping events are independent the problem can be seen as a random walk in accumulated repumping time. Each step of this random walk is then exponentially distributed around the mean repumping time τ_{reset} . The probability distribution of the summed repumping time is given by³⁰

$$P_{ek} = \frac{t'^{k-1}}{\tau_{reset}^k (k-1)!} e^{-t'/\tau_{reset}} \approx \frac{1}{\sigma\sqrt{2\pi}} e^{-\frac{(t' - \mu)^2}{2\sigma^2}} \quad (5.3)$$

where we use the central limit theorem to approximate this distribution by a normal distribution with width $\sigma = \tau_{reset}\sqrt{k}$ and mean $\mu = \tau_{reset}k$, as we are interested in solutions for a large number of repumping events. The expected fidelity after N experimental runs is calculated by summing over the probability distributions for the electronic state and the corresponding accumulated repumping time

$$\begin{aligned} F_N &= \sum_{k=0}^N P_{ek} \int F_k P_{ek} dt' \\ &= \frac{1}{2} + \frac{1}{2} \sum_{k=0}^N P_{ek} e^{-\frac{1}{2}k\tau_{reset}^2 d\omega^2} \\ &= \frac{1}{2} + \frac{1}{2^{N+1}} \left(1 + e^{-\frac{1}{2}\tau_{reset}^2 d\omega^2}\right)^N \end{aligned}$$

References

- [1] W. B. Gao, A. Imamoglu, H. Bernien and R. Hanson. Coherent manipulation, measurement and entanglement of individual solid-state spins using optical fields. *Nature Photonics* **9**, 363 (2015).
- [2] H. J. Kimble. The quantum internet. *Nature* **453**, 1023 (2008).
- [3] D. L. Moehring et al. Entanglement of single-atom quantum bits at a distance. *Nature* **449**, 68 (2007).
- [4] S. Ritter et al. An elementary quantum network of single atoms in optical cavities. *Nature* **484**, 195 (2012).
- [5] J. Hofmann et al. Heralded entanglement between widely separated atoms. *Science* **337**, 72 (2012).
- [6] H. Bernien et al. Heralded entanglement between solid-state qubits separated by three metres. *Nature* **497**, 86 (2013).
- [7] C. H. Bennett et al. Purification of noisy entanglement and faithful teleportation via noisy channels. *Physical Review Letters* **76**, 722 (1996).
- [8] E. T. Campbell and S. C. Benjamin. Measurement-based entanglement under conditions of extreme photon loss. *Physical Review Letters* **101**, 130502 (2008).
- [9] H.-J. Briegel, W. Dür, J. I. Cirac and P. Zoller. Quantum repeaters: The role of imperfect local operations in quantum communication. *Physical Review Letters* **81**, 5932 (1998).
- [10] L. Childress, J. M. Taylor, A. S. Sørensen and M. D. Lukin. Fault-tolerant quantum communication based on solid-state photon emitters. *Physical Review Letters* **96**, 070504 (2006).
- [11] L. Childress and R. Hanson. Diamond NV centers for quantum computing and quantum networks. *MRS Bulletin* **38**, 134 (2013).
- [12] E. Togan et al. Quantum entanglement between an optical photon and a solid-state spin qubit. *Nature* **466**, 730 (2010).
- [13] W. Pfaff et al. Unconditional quantum teleportation between distant solid-

- state quantum bits. *Science* **345**, 532 (2014).
- [14] F. Jelezko et al. Observation of coherent oscillation of a single nuclear spin and realization of a two-qubit conditional quantum gate. *Physical Review Letters* **93**, 130501 (2004).
- [15] M. V. G. Dutt et al. Quantum register based on individual electronic and nuclear spin qubits in diamond. *Science* **316**, 1312 (2007).
- [16] P. Neumann et al. Multipartite entanglement among single spins in diamond. *Science* **320**, 1326 (2008).
- [17] B. Smeltzer, J. McIntyre and L. Childress. Robust control of individual nuclear spins in diamond. *Physical Review A* **80**, 050302 (2009).
- [18] G. D. Fuchs, G. Burkard, P. V. Klimov and D. D. Awschalom. A quantum memory intrinsic to single nitrogen-vacancy centres in diamond. *Nature Physics* **7**, 789 (2011).
- [19] T. van der Sar et al. Decoherence-protected quantum gates for a hybrid solid-state spin register. *Nature* **484**, 82 (2012).
- [20] T. H. Taminiau et al. Detection and control of individual nuclear spins using a weakly coupled electron spin. *Physical Review Letters* **109**, 137602 (2012).
- [21] P. C. Maurer et al. Room-temperature quantum bit memory exceeding one second. *Science* **336**, 1283 (2012).
- [22] A. Laraoui et al. High-resolution correlation spectroscopy of ^{13}C spins near a nitrogen-vacancy centre in diamond. *Nature Communications* **4**, 1651 (2013).
- [23] P. Tamarat et al. Spin-flip and spin-conserving optical transitions of the nitrogen-vacancy centre in diamond. *New Journal of Physics* **10**, 045004 (2008).
- [24] L. Robledo et al. High-fidelity projective read-out of a solid-state spin quantum register. *Nature* **477**, 574 (2011).
- [25] S. Kolkowitz, Q. P. Unterreithmeier, S. D. Bennett and M. D. Lukin. Sensing distant nuclear spins with a single electron spin. *Physical Review Letters* **109**, 137601 (2012).
- [26] N. Zhao et al. Sensing single remote nuclear spins. *Nature Nanotechnology* **7**, 657 (2012).
- [27] T. H. Taminiau, J. Cramer, T. v. d. Sar, V. V. Dobrovitski and R. Hanson. Universal control and error correction in multi-qubit spin registers in diamond. *Nature Nanotechnology* **9**, 171 (2014).

- [28] S. D. Barrett and P. Kok. Efficient high-fidelity quantum computation using matter qubits and linear optics. *Physical Review A* **71**, 060310 (2005).
- [29] M. Doherty et al. The nitrogen-vacancy colour centre in diamond. *Physics reports* **528**, 1-45 (2013).
- [30] M. Akkouchi. On the convolution of exponential distributions. *Journal of the Chungcheong mathematical society* **21**, 4 (2008).

Acknowledgements

We thank C. Degen and M. Loretz for useful discussions. We acknowledge support from the Dutch Organization for Fundamental Research on Matter (FOM), the Netherlands Organization for Scientific Research (NWO), the Defense Advanced Research Projects Agency QuASAR program, and the European Research Council through a Starting Grant. THT is supported by a NWO VENI grant.

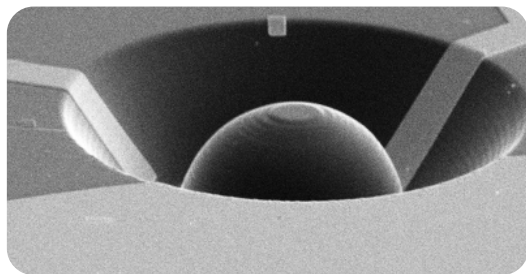
Figure 1. The NV-center as a network node including a quantum memory. A single electron spin (orange) is coupled (purple curly arrows) to individual carbon spins (blue) via the magnetic dipole field (black dashed lines) associated with the electron spin. A laser beam (red straight arrow) is used to prepare and read-out the spin state by collecting the fluorescence (red curly arrow). (a) Scanning electron microscope image of the sample. A solid-immersion lens is fabricated with a focused ion beam in single-crystalline diamond for high collection efficiency. An on-chip gold stripline (bottom) enables microwave-control. (b) Level scheme for the quantum memory (^{13}C -spin, $I = 1/2$). The hyperfine coupling introduces energy level splittings (ω_0 and ω_1) that depend on the state of the electron spin, where $\omega_0 = (2\pi) \gamma_c B$ with γ_c the gyromagnetic ratio of the carbon spin and B the magnetic field and ω_1 depends on the hyperfine coupling, which is set by the distance to the electron spin. (c) Relevant ground-state energy levels of the electron spin ($S = 1$). The degeneracy of the $m_s = \pm 1$ states is lifted by applying a magnetic field along the quantization axis of the NV-center. We define the electron spin qubit in the $|0\rangle = |m_s = 0\rangle$, $|1\rangle = |m_s = +1\rangle$ manifold. Here $B_z = (303 \pm 1)$ G leading to an energy level splitting $\omega_e \sim (2\pi) 3.73\text{GHz}$. (d) Diagram of the electron spin including the relevant ground-, and excited-state levels. At low temperature the zero phonon line (~ 637 nm) exhibits spin-preserving optical transitions that can be addressed selectively. In the experiment, two lasers with different frequency are used to address the E' transition for electron spin initialization (dashed red) and the E_y transition for readout (fidelity = 0.93(5)) and generating spin-photon entanglement (solid red).

Figure 2. Characterization of single ^{13}C spins. (a) Circuit diagram to determine ω_0 and ω_1 of individual ^{13}C spins via the electron spin. The conditional gates on the carbon spin are implemented using resonant dynamical decoupling techniques as explained in the main text. Because the evolution of the carbon spin is correlated with an eigenstate of the electron spin during the interference, a coherent signal can be observed even for $\tau \gg T_{2,electron}^* = (4.18 \pm 0.01) \mu\text{s}$ (b)-(e) The resulting interference signal measured for four individual ^{13}C spins near a single NV-center. Grey lines are fits to the data with function $F = \frac{A}{2}\cos(\omega_0\tau + \phi_0) + \frac{B}{2}\cos(\omega_1\tau + \phi_1) + c$. We find $\omega_0/2\pi = (326.0 \pm 0.2), (325.9 \pm 0.2), (325.1 \pm 0.5), (325.9 \pm 0.4)$ kHz (b-e), consistent with the gyromagnetic ratio of a ^{13}C spin in a field of (303 ± 1) G. For the second frequency component we find $\omega_1/2\pi = (364.6 \pm 0.1), (293.7 \pm 0.2), (354.7 \pm 0.5), (371.5 \pm 0.4)$ kHz. The data is taken with 500 repetitions per data point and the error bars correspond to one standard deviation.

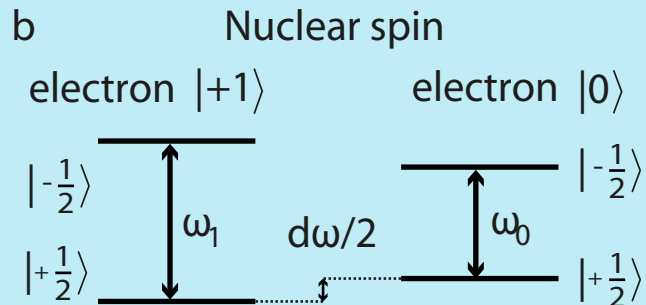
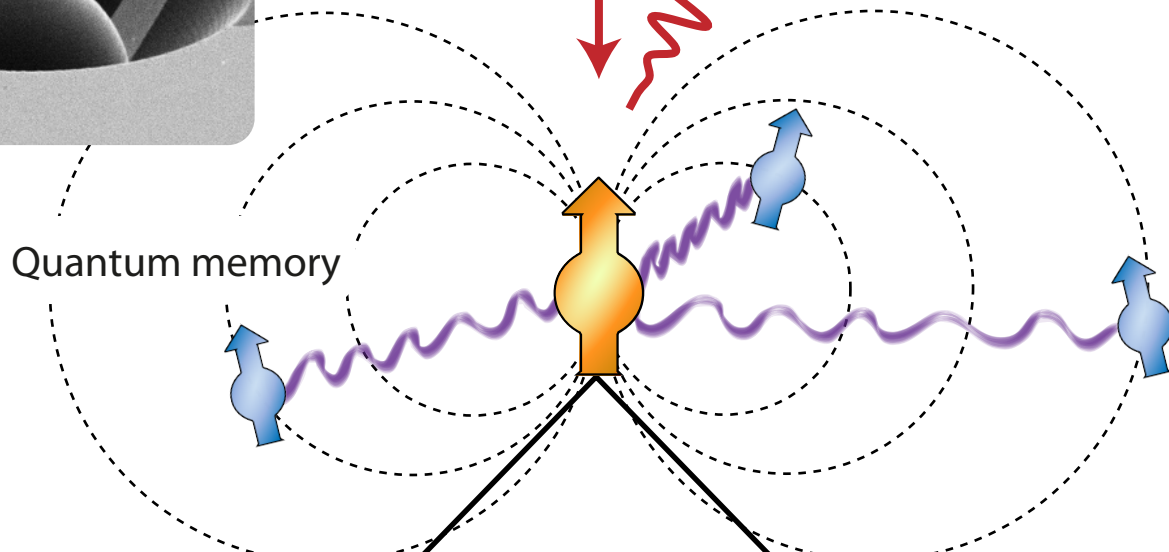
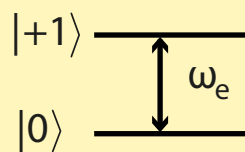
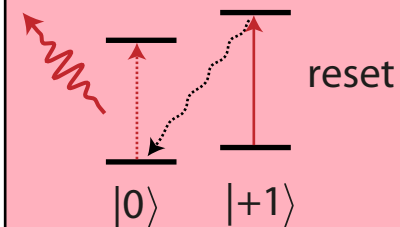
Figure 3. Simulations of the dephasing of a ^{13}C spin quantum memory while generating entanglement. (a) Diagram for the protocol to create spin-photon entanglement. (b) Simulations of the fidelity for different ^{13}C spins after $N=50$ repetitions of the protocol, assuming that the reset is instantaneous ($t'=0$, formula 3.1 of main text). The initial state of a carbon spin can be perfectly preserved by choosing the time between the $\pi/2$ -pulse and the reset to $t = 2\pi / d\omega$. (c) The effect of the spin pumping process on the fidelity of the memory after $N=50$ repetitions. Orange dots are a Monte-Carlo simulation where for every electron spin reset, a time t' is drawn from an exponential probability distribution with $\tau_{reset} = 390 \text{ ns}$. Grey line is a comparison with an ideal reset. $d\omega = (2\pi) 38.6 \text{ kHz}$. (d) Dependence of the memory fidelity on the characteristic reset time τ_{reset} using formula 3.2. (e) Dephasing of the memory as a function of entanglement attempts for different coupling strengths, fixing $\tau_{reset} = 1 \mu\text{s}$.

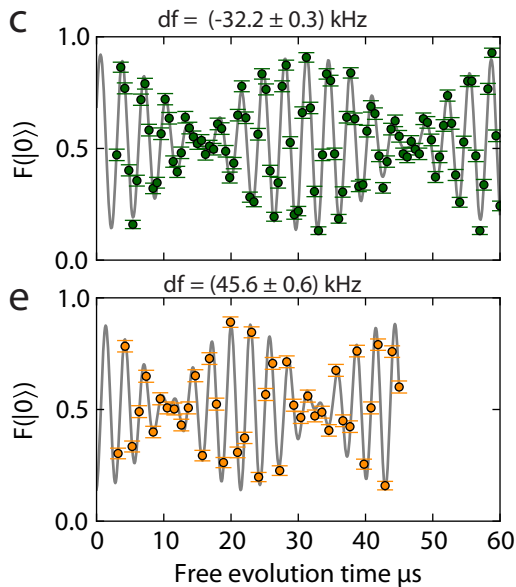
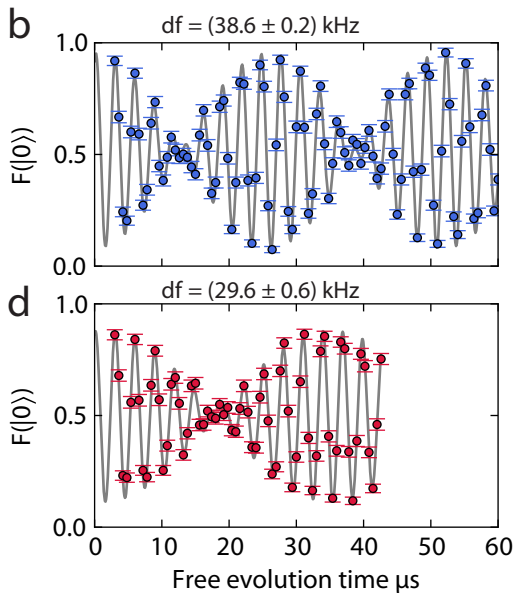
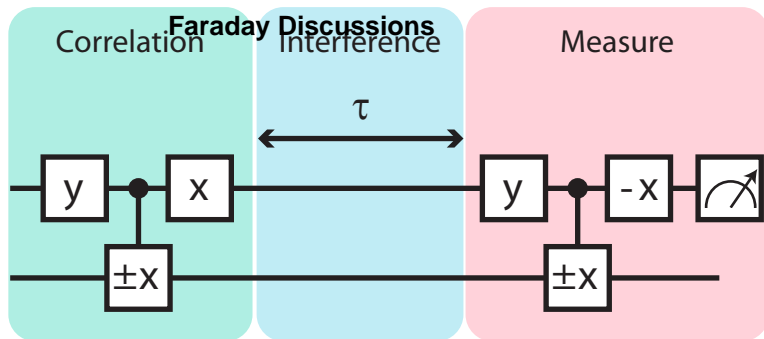
Faraday Discussions

a

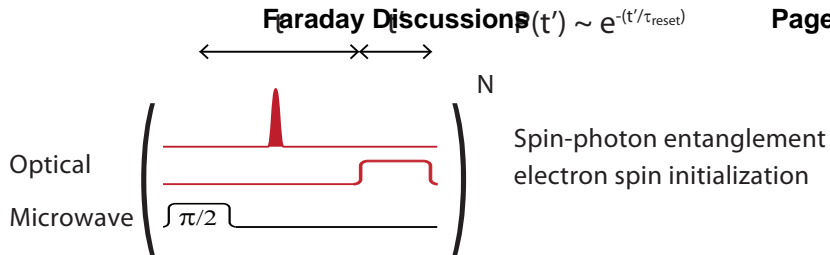


Quantum memory

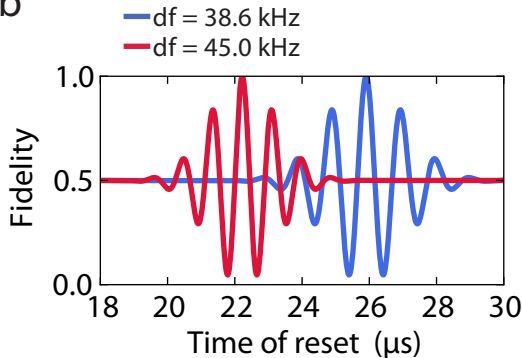
**c Electron spin****d Photonic interface**



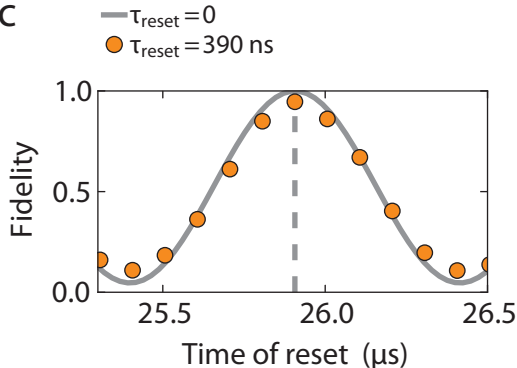
a



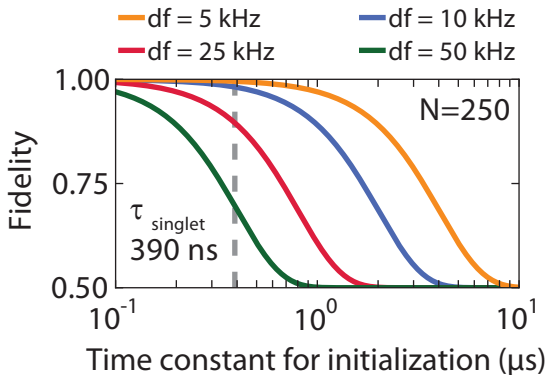
b



c



d



e

